Determination of low latitude plasma drift speeds from FUV images

Thomas J. Immel, Stephen B. Mende, Harald U. Frey, and Laura M. Peticolas
Space Sciences Laboratory, University of California, Berkeley, USA

Eiichi Sagawa
Communications Research Laboratory, Tokyo, Japan

Received 21 April 2003; revised 19 June 2003; accepted 24 July 2003; published 24 September 2003.

[1] Thousands of images of the nighttime equatorial airglow arcs have been obtained by the Far-Ultraviolet Imager (FUV) on-board the NASA IMAGE satellite. Imaging periods lasting several hours around the time of satellite apogee allow for the determination of the velocity of drifting plasma density depletions occurring within the airglow arcs. These velocities reflect the $\mathbf{E} \times \mathbf{B}$ drift of low-latitude plasma under the influence of a vertical electric field. A survey of several weeks of data produces information regarding the variation of drift speeds with solar 10.7-cm radio flux. Comparisons to previous measurements by the Jicamarca radar show that the FUV-determined plasma drift speeds are 10–35% greater, particularly before 2100 local time. This difference is attributed mainly to the different magnetic latitudes of the observations. *INDEX TERMS:* 2415 Ionosphere: Equatorial ionosphere; 0310 Atmospheric Composition and Structure: Airglow and aurora; 2437 Ionosphere: Ionospheric dynamics; 0394 Atmospheric Composition and Structure: Instruments and techniques; 2439 Ionosphere: Ionospheric irregularities. **Citation:** Immel, T. J., S. B. Mende, H. U. Frey, L. M. Peticolas, and E. Sagawa, Determination of low latitude plasma drift speeds from FUV images, *Geophys. Res. Lett.*, *30*(18), 1945, doi:10.1029/2003GL017573, 2003.

1. Introduction

[2] The terrestrial equatorial airglow arcs, like the auroral ovals, are persistent features of Earth's far-ultraviolet (FUV) signature [*Carruthers and Page*, 1976]. The arcs appear as a pair of emission bands on both sides of Earth's magnetic equator, extending from the dusk terminator eastward across the nightside. Unlike the aurora, their intensity does not indicate the strength or rate of coupling to the magnetosphere, but rather the state of the equatorial ionosphere [*Sojka*, 1991]. The arcs indicate regions of enhanced ionospheric densities where ionospheric plasma is concentrated after rising from the magnetic equator under the influence of daytime dynamo electric fields. The concentration occurs as the plasma diffuses along magnetic field lines that direct plasma downward and to the north and south of the magnetic equator [*Hanson and Moffett*, 1966]. Due to the complex interaction of the ionosphere and thermosphere in the low-latitude evening sector, localized instabilities can rapidly grow in altitude, resulting in strong localized depletions in plasma densities with corresponding decreases in airglow brightness in the airglow arcs [*Weber et al.*, 1978]. From years of observations by radars based at low latitudes come the terms "spread-F" to describe the conditions of the destabilized F-region, and "bubbles" or "plumes" to describe the ionospheric depletion associated with the fully developed spatial instability, which is the cause of the large-scale airglow depletions [*Kelley*, 1989].

[3] New global scale studies of these phenomena are now possible using the spectrographic imaging component of the Far-Ultraviolet Imager (FUV) on the IMAGE satellite [*Burch*, 2000; *Mende et al.*, 2000a]. In this study the SI-13 channel is used, which, with its 5-nm passband centered at 135.6 nm, is specifically designed for observations of that emission of atomic oxygen [*Mende et al.*, 2000b]. For auroral or dayside studies, care must be taken to interpret the images with the knowledge that particular bands of the Lyman Birge Hopfield (LBH) emission of N_2 also lie in the imager's passband. Because the LBH emission is only produced by direct impact of ~10 eV electrons on N_2, either photoelectrons or secondary auroral electrons, it is generally not produced at low latitudes on the nightside and does not contribute to the SI-13 signal during these observations.

2. IMAGE Observations

[4] The IMAGE satellite was placed in a highly elliptical orbit (perigee altitude = 1000 km, apogee altitude = 7.2 R_E) in March of 2000. Apsidal motion of the orbit has caused the latitude of apogee to proceed from 40° to 90° and back down to cross the equator in early 2003. In March 2002, the latitude was sufficiently low to consistently view the northern equatorial airglow arc, with improved viewing of the southern arc by May. It is during these months with the local time of apogee is in the evening sector, providing a clear view of the airglow arc from the evening terminator to post-midnight local times. The FUV imaging cadence matches the 2-minute rotation period of the satellite, with 5 seconds of integration time per SI-13 image.

[5] Two imaging examples, obtained at 1141 and 1417 UT on Day 87 (March 28), 2002, are shown in Figure 1. Though the latitude of the satellite moves from 53.7° to 64.9°, the northern equatorial airglow arc remains visible. Furthermore, the arc brightens over the time period, with brightnesses >300 Rayleigh (R) extending to the midnight sector and over a broader range of magnetic latitudes. The conversion to brightness from instrument counts is performed according to the UV stellar calibration of the instrument described by *Frey et al.* [2003].

3. Analysis Technique

[6] In order to observe the development of spatial and temporal variations in the arc's brightness, full sequences of

0094-8276/03/2003GL017573$05.00

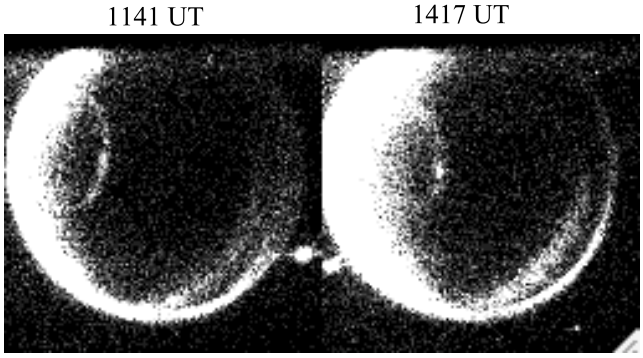

Figure 1. A pair of 135.6-nm images of Earth obtained by the SI-13 instrument on March 28, 2002 (day 87) at 1141 and 1417 UT.

images must be examined. To do this, all the images obtained during observing intervals of interest are remapped to a regularly spaced grid of magnetic local time (MLT) and latitude (MLat), and the instrument counts between 0 and 25° MLat are added to report a single number for each 0.5° increment of MLT [see also *Sagawa et al.*, 2003 for further use of this technique]. The data set that results can be presented as a keogram, with UT on the vertical axis and MLT on the horizontal axis. The keogram reveals the relative MLT motion of brightness irregularities as a function of UT. For this work, the APEX magnetic coordinate system is used [*Richmond*, 1995].

[7] The MLT-UT keogram for the imaging interval including the images of Figure 1 is shown in Figure 2a. The decreases in total 135.6-nm emission intensity in the airglow arc are revealed in this presentation by the several dark tracks that advance in MLT with increasing UT. This keogram clearly shows the development of 5 depleted regions which cross the 20 hours MLT sector at 1050, 1140, 1255, 1310, and 1340 UT. There is also a traveling enhancement in brightness that crosses the 20 hours MLT sector around 1230. In terms of development of spread-F in the evening sector, this is an active period with instabilities growing into multiple large plumes in <4 hours time.

[8] These data from the same imaging interval are replotted in a co-rotating frame of reference in Figure 2b. The horizontal axis now shows the magnetic longitude (MLon) of the FUV measurements during the same time period as in Figure 2a. Features fixed with respect to locations on the ground would appear as vertical traces in this display. For reference, the 20 MLT position is indicated with a solid line, decreasing in longitude with time. As in the previous plot, the FUV brightness decreases are obvious and now clearly demonstrate a drift toward greater longitudes (eastward). What is also clear from the pair of plots in Figure 2 is that the drifts are most rapid at early evening local times, slowing down by a factor of 2 or more by midnight. The first three depletions to pass through the 20 MLT sector are indicated in each panel of Figure 2, and they will now be further analyzed.

[9] To determine the drift speed of individual plasma depletions, the MLon and UT of the center of the depletion is determined at 15 points in the keogram, and a least-squares fit to the points is determined using a 4th degree polynomial. The derivative of the fit is then calculated, giving the fitted instantaneous drift speed of the depletion over the time of observation. The calculated speeds are subsequently converted from MLon/sec to absolute ground speed in m/sec, a correction of up to 15%. This method is applied for the 3 separate depletions indicated in Figure 2, and the results are shown in Figure 3. Plotted now with UT on the abscissa, the position as a function of time for the 3 depletions is shown in Figure 3a, with the polynomial fits overlaid. The derivatives of the 3 fits are shown in Figure 3b, which show the instantaneous drift speed as a function of

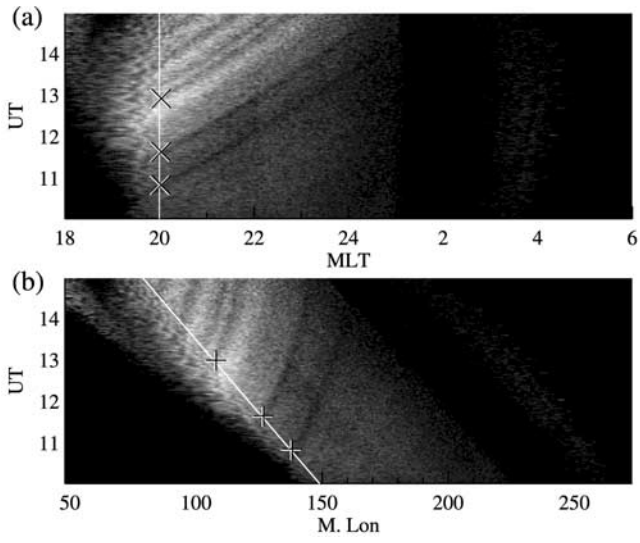

Figure 2. Magnetic Local Time and Longitude keograms of Day 87, 2002, SI-13 imaging period. (a) MLT-UT keogram, showing advance of 135.6-nm O I brightness depressions in local time. (b) Mag. Longitude-UT keogram, showing advance of brightness depressions in magnetic longitude. In each plot the 20 MLT location is indicated with a solid line, on which the crossing times of 3 significant depletions is marked.

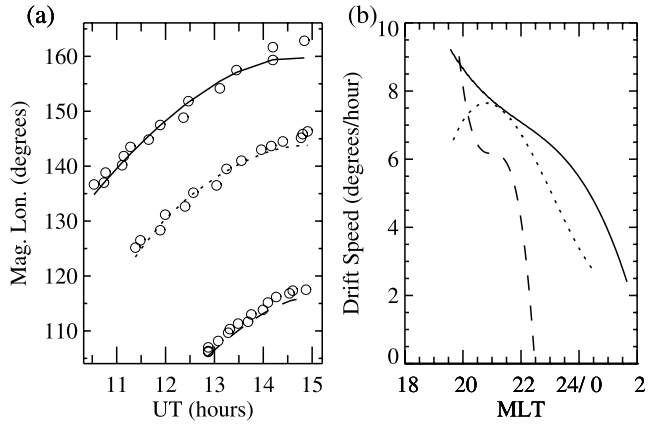

Figure 3. Drift data fitted to determine drift velocity (a) The track of three of the brightness decreases from Figure 2b in UT vs. MLon, with 4-th degree polynomial fits overlaid. (b) Speed of the brightness depletions in degrees per hour. Solid, dotted, and dashed lines are used to separately indicate each of the three traces from Figure 3a.

MLT. The speeds are greatest in early evening, with values between 6 and 9 degrees/hour in the 20 MLT sector.

[10] This technique is applied to outstanding plasma depletions observed from days 87–129, 2002, and the resulting average drift speeds from 94 samples are shown in Figure 4. These data are actually separated into two groups by the daily 10.7-cm solar flux values ($F_{10.7}$), which serves as a proxy for the solar EUV flux [*Hedin*, 1984]. The median and mean for the data set are both ~190 Jy, so that value is selected to separate the groups, with mean $F_{10.7}$ values of 171 and 208 Jy in the low and high flux bins, respectively. It is logical to expect a solar flux effect, as greater heating on the dayside drives greater thermospheric neutral winds, which in turn generate greater dynamo electric fields and plasma drifts at low latitudes [*Biondi et al.*, 1991, 1999]. Though both sets show the same general trend with a peak at 20 MLT and decreasing values thereafter, the high solar flux drift speeds ('x' marks) are ~40 m/sec greater at their peak than the low flux speeds (squares). They remain higher until about 23 MLT.

[11] Also shown in Figure 4 are values for equinox plasma drift speeds determined using the ground-based radar at Jicamarca. These data, taken directly from Figure 7 of *Fejer et al.* [1991], are also organized by $F_{10.7}$, with average values of 78, 123, and 204 Jy. The trend towards faster drifts with increasing solar radio flux is apparent in these data as well. Comparing the high flux drift speeds from both data sets, one may note that the overall drift speeds determined from space are generally 10–20% greater than the radar determined values, with up to a 35% enhancement of peak velocities.

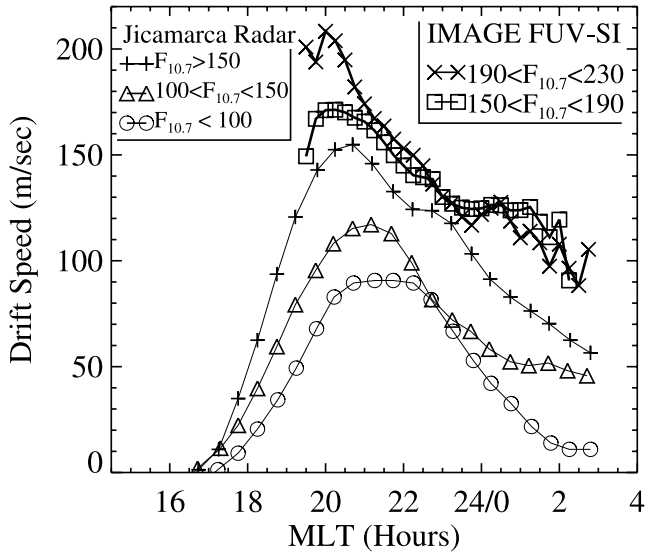

Figure 4. Average plasma drift velocities across the nightside for >40 days in 2002. The eastward velocity of identifiable plasma depletions is determined as shown in Figure 3 for every IMAGE observational period between days 82 and 129, 2002. These data are separated into two ranges of $F_{10.7}$, where the separation of 190 Jy is the mean value for all the observations. Shown for comparison (in 3 bins of $F_{10.7}$) are averaged data from the Jicamarca radar described by *Fejer et al.* [1991].

4. Discussion

[12] The difference between the ground- and space-based data presented in Figure 4 is significant. It raises the question of whether the radar and imaging techniques are comparable. However, good agreement has been reported between plasma drift speeds determined by radars and from optical tracking of drifting depletions [*Mendillo et al.*, 1997]. Considering that the space-based technique used in this report is similar to the ground-based technique, good correspondence between optically observed plasma drift speeds and the average drift speed of the plasma is expected.

[13] The main difference in the measurements is that the Jicamarca radar and IMAGE/FUV instrument are not measuring plasma drifts at the same latitude. The technique developed here integrates all observations along magnetic meridians between 0 and 25° MLat, where Jicamarca radar observations are confined to ±5°. Since the greatest FUV emissions are usually around 10–15° MLat, most of the signal comes from areas out of the range of the Jicamarca radar. Recent research results have shown that plasma in the vicinity of the equatorial ionospheric anomaly can have a larger eastward speed than would be expected if one referred to averages determined using the Jicamarca radar [*Kil et al.*, 2000]. Earlier space-based electric field measurements also suggested that the maximum eastward drifts are more likely to be found at ±8° MLat [*Aggson et al.*, 1987]. These results agree with the IMAGE/FUV observations discussed here but conflict with other low latitude measurements, which show greater drift speeds at the equator than in the anomaly [e.g., *Basu et al.*, 1996].

[14] Very recent results using dual all-sky imaging of plasma depletions across 15° of latitude, and numerical simulations of the ionospheric E and F regions suggest a resolution to the contradiction [*Martinis et al.*, 2003]. That research demonstrates that the local time is an important factor, and that eastward drift speeds at 10–15° MLat are expected to exceed speeds at the magnetic equator until late evening (~2230 LT). By tracking airglow depletions, *Martinis et al.* found the average plasma drift speeds at −14° MLat to be greater than at the equator by nearly 100% at 2100 LT. Though the FUV observations exceed Jicamarca averages by only as much as 35%, the largest difference is in the 2100 LT sector, consistent with the results of *Martinis et al.*. That the FUV speeds continue to exceed the radar average speeds after 2400 LT presents a question for further investigation.

5. Conclusion

[15] This paper describes the first space-based FUV observations of drifting low-latitude plasma depletions. A technique has been developed to allow for the determination of the zonal drift speed by tracking the depletions. A modulation of the solar $F_{10.7}$ index by 80 Jy in the 5 weeks of observation manifests itself as a ~40 m/sec variation in the peak nightside plasma drift speed. Comparing to earlier ground based work on the importance of the solar input on drift speeds, this variation is of the magnitude expected for the given change in solar flux. The local time variation, with a peak speed around 20 MLT and a gradual decrease until midnight, compares well with several ground based studies

of low latitude plasma drifts, though the IMAGE/FUV determined drift speeds exceed average speeds determined with the Jicamarca radar by 10–35%. A latitudinal-local time variation of the plasma drift speed is cited as the most probable explanation of the difference.

[16] Further observations in 2003 and 2004, including direct conjugate observations of the southern arc, will be useful in addressing the question of plasma bubble frequency vs. magnetic activity. Also, the degree of conjugacy of the arcs during equinox conditions will be important for discussions of high-latitude effects on the equatorial ionosphere. Observation of the development of plasma density decreases associated with spread-F and the simultaneous determination of plasma drift speeds across the active evening ionosphere could prove to be a significant new contribution to the mature field of equatorial ionospheric physics.

[17] **Acknowledgments.** IMAGE FUV analysis is supported by NASA through Southwest Research Institute subcontract number 83820 at the University of California, Berkeley, contract NAS5-96020.

References

Aggson, T. L., N. C. Maynard, F. A. Herrero, H. G. Mayr, L. H. Brace, and M. C. Liebrecht, Geomagnetic equatorial anomaly in zonal plasma flow, *J. Geophys. Res.*, *92*, 311–315, 1987.

Basu, S., et al., Scintilations, plasma drifts, and neutral winds in the equatorial ionosphere after sunset, *J. Geophys. Res.*, *101*, 26,795–26,809, 1996.

Biondi, M. A., J. W. Meriwether, B. G. Fejer, S. A. Gonzales, and D. C. Hallenbeck, Equatorial thermospheric wind changes during the solar cycle measurements at Arequipa, Peru, from 1983 to 1990, *J. Geophys. Res.*, *96*, 15,917–15,930, 1991.

Biondi, M. A., S. Y. Sazykin, B. G. Fejer, J. W. Meriwether, and C. G. Fesen, Equatorial and low latitude thermospheric winds: Measured quiet time variations with season and solar flux from 1980 to 1990, *J. Geophys. Res.*, *104*, 17,091–17,106, 1999.

Burch, J. L., IMAGE mission overview, *Space Sci. Rev.*, *91*, 1–14, 2000.

Carruthers, G. R., and T. Page, Apollo 16 far ultraviolet imagery of the polar auroras, tropical airglow belts, and general airglow, *J. Geophys. Res.*, *81*, 483–496, 1976.

Fejer, B. G., E. R. de Paula, S. A. González, and R. F. Woodman, Average vertical and zonal F region plasma drifts over Jicamarca, *J. Geophys. Res.*, *96*, 13,901–13,906, 1991.

Frey, H. U., et al., Summary of quantitative interpretation of IMAGE far ultraviolet auroral data, *Space Sci. Rev.*, in press, 2003.

Hanson, W. B., and R. J. Moffett, Ionization transport effects in the equatorial F region, *J. Geophys. Res.*, *71*, 5559, 1966.

Hedin, A. E., Correlations between thermospheric density and temperature, solar EUV flux, and 10.7-cm flux variations, *J. Geophys. Res.*, *89*, 9828–9834, 1984.

Kelley, M. C., *The Earth's Ionosphere Plasma Physics and Electrodynamics*, Academic Press, Inc., San Diego, 1989.

Kil, H., P. M. Kintner, E. R. de Paula, and I. J. Kantor, Global Positioning System measurements of the ionospheric zonal apparent velocity at Cachoeira Paulista in Brazil, *J. Geophys. Res.*, *105*, 5317–5327, 2000.

Martinis, C., J. V. Eccles, J. Baumgardner, J. Manzano, and M. Mendillo, Latitude dependence of zonal plasma drifts obtained from dual-site airglow observations, *J. Geophys. Res.*, *108*, 1129, doi:10.1029/2002JA009462, 2003.

Mende, S. B., et al., Far ultraviolet imaging from the IMAGE spacecraft. 1. Systems design, *Space Sci. Rev.*, *91*, 243–270, 2000a.

Mende, S. B., et al., Far ultraviolet imaging from the IMAGE spacecraft. 3. Spectral imaging of Lyman-α and OI 135.6 nm, *Space Sci. Rev.*, *91*, 287–318, 2000b.

Mendillo, M., J. Baumgardner, M. Colerico, and D. Nottingham, Imaging science contributions to equatorial aeronomy: Initial results from the MISETA program, *J. Atmos. Solar-Terr. Phys.*, *59*, 1587–1599, 1997.

Richmond, A. D., Ionospheric electrodynamics using magnetic apex coordinates, *J. Geomagn. Geoelectr.*, *47*, 191–212, 1995.

Sagawa, E., T. Maruyama, T. J. Immel, H. U. Frey, and S. B. Mende, Global view of the nighttime low latitude ionosphere by the 135.6 nm OI observation with IMAGE/FUV, *Geophys. Res. Lett.*, *30*, 1534, doi:10.1029/2003GL017140, 2003.

Sojka, J. J., Ionospheric physics, *Rev. Geophys*, *29*, 1166–1186, 1991.

Weber, E. J., J. Buchau, R. H. Eather, and S. B. Mende, North-south aligned equatorial airglow depletions, *J. Geophys. Res.*, *83*, 712–716, 1978.

T. J. Immel, S. B. Mende, H. U. Frey, and L. M. Peticolas, Space Sciences Laboratory, University of California, Berkeley, CA 94720, USA. (immel@ssl.berkeley.edu)

E. Sagawa, Communications Research Laboratory, Tokyo, Japan. (esagawa@crl.go.jp)